The Sparse Data Extrapolation Problem: Strategies for Soft-Tissue Correction for Image-Guided Liver Surgery

Michael I. Miga[a*], Prashanth Dumpuri[b], Amber L. Simpson[a], Jared A. Weis[a], and William R. Jarnagin[c]
[a]Vanderbilt University, Department of Biomedical Engineering, Nashville, TN, USA,
[b]Pathfinder Therapeutics Inc., Nashville, TN, USA,
[c]Memorial Sloan-Kettering Cancer Center, Department of Surgery - Hepatopancreatobiliary Service, New York, NY, USA
*corresponding author

ABSTRACT

The problem of extrapolating cost-effective relevant information from distinctly finite or sparse data, while balancing the competing goals between workflow and engineering design, and between application and accuracy is the 'sparse data extrapolation problem'. Within the context of open abdominal image-guided liver surgery, one realization of this problem is compensating for non-rigid organ deformations while maintaining workflow for the surgeon. More specifically, rigid organ-based surface registration between CT-rendered liver surfaces and laser-range scanned intraoperative partial surface counterparts resulted in an average closest-point residual 6.1 ± 4.5 mm with maximum-signed distances ranging from -13.4 to 16.2 mm. Similar to the neurosurgical environment, there is a need to correct for soft tissue deformation to translate image-guided interventions to the abdomen (e.g. liver, kidney, pancreas, etc.). While intraoperative tomographic imaging is available, these approaches are less than optimal solutions to the sparse data extrapolation problem. In this paper, we compare and contrast three sparse data extrapolation methods to that of data-rich interpolation for the correction of deformation within a liver phantom containing 43 subsurface targets. The findings indicate that the subtleties in the initial alignment pose following rigid registration can affect correction up to 5-10%. The best deformation compensation achieved was approximately 54.5% (target registration error of 2.0 ± 1.6 mm) while the data-rich interpolative method was 77.8% (target registration error of 0.6 ± 0.5 mm).

Keywords: liver, image-guided surgery, finite element, deformation correction, elasticity, biomechanics, model

1. INTRODUCTION

Hepatic tumors represent an important health care problem in the U.S. [1]. Along with hepatocellular cancer (which represents only 4% of primary cancers in the US, however, worldwide is far more prevalent [2]), many primary neoplasms metastasize to the liver which is the significant presentation. Depending on the treatment center, about 72% of malignant tumors in the liver are metastatic, and approximately 69% of metastases derive from colorectal carcinoma. In fact, the most common tumor treated in the liver is metastatic colorectal carcinoma (MCRC), a condition where hepatic metastasectomy can result in long-term survival in properly selected patients. Considering that approximately 140,000+ new cases of colorectal cancer will be diagnosed this year [1], with approximately 60% [3] developing metastatic liver disease, the impact of a system that facilitates liver resection would be profound. Recent reports have demonstrated that increased and more aggressive hepatic resections have improved five year survival rates for patients with MCRC [4-6]. In one study specifically grouping subjects according to extent of resection, five year survival rates rose from 38% to 45% with no increase in complication rate [6]. Unfortunately, the patient population eligible for resective therapy is limited. Based on one study involving 2400 subjects presenting with MCRC, only 20% of patients were eligible for surgical resection [5]. This discrepancy may result from many factors, but is likely influenced by the magnitude and complexity of hepatic resections as they are currently performed. Interestingly, non-surgical treatments are being proposed as an adjuvant with an aim to down-stage metastases to achieve resection candidacy [7]. Increasing the number of patients eligible for liver resection therapy by providing enhanced guidance will have direct impact on survival for a large population of patients. The choice seems clear; however, as more aggressive liver procedures are performed (multi-segment or lobectomy procedure) complication rates increase. So while liver resection has shown

promising survival rates and a perioperative mortality rate of less than 5%, a significant increase in postoperative morbidity due to hepatic dysfunction and infection has also been reported, even by specialized centers [8, 9]. In one recent study, postoperative complications doubled when comparing major to minor hepatectomy procedures [10]. The translation of accurate image-guided surgical therapy for open abdominal procedures is a mission critical tool for breaking down these surgical barriers and increasing the possibility of favorable outcomes for more patients undergoing this aggressive and complex procedure.

In the past, the translation of image-guided surgery techniques to the abdominal environment has been limited. The most widely used approaches are active imaging with the use of ultrasound (US) or laparoscopic imaging. Preoperative imaging and planning data integrated for active intraoperative guidance is not commonplace [11-14] and only until recently has become commercialized through our industrial collaborator, Pathfinder Therapeutics Inc. (PTI) (Nashville, TN, USA). The difficulty that arises when attempting full scale integration is the presence of soft-tissue deformation. In recent reports, soft tissue deformation during liver resection has been documented with intraoperative computed tomography (iCT) and has demonstrated significant effects [15]. While intraoperative magnetic resonance (iMR) and iCT are available, these approaches are cumbersome, incur radiation dose in the latter, and are not economically scalable to mid-level medical centers. The work by Lange et al. [14, 16, 17] is looking at a CT-to-US vessel based non-rigid registration system for providing the link between image and physical space. While the 3 cases reported performed well, the likelihood of this approach working within the confines of OR workflow is a challenge. In addition, it requires the identification of as many bifurcations as possible with tracked ultrasound and then the determination of corresponding bifurcations within the CT. While the subsurface information would be valuable for non-rigid correction, there is a likelihood of misidentification in this highly vascularized organ, and the encumbrance may challenge adoption.

Given the nature of the procedure, the need to compensate for deformation is evident but as the nature of resection is unlike its neurosurgical counterpart, the requirements of compensation need to be balanced with workflow and accuracy requirements. Presentation for open liver surgery (and even laparoscopic to a degree) involves significant organ distortion prior to the ability to collect data, but does afford considerable exposure for understanding that presentation. Because the liver regenerates, the margins for surgical resection are more liberal but understanding the local vascular environment is critical. These surgical characteristics serve as constraints to data acquisition and guidance procedure execution. These constraints are the foundation of the ‘sparse data extrapolation problem’. More specifically, the problem of extrapolating cost-effective relevant information from distinctly finite or sparse data while balancing the competing goals between workflow and engineering design, and between application and accuracy is the ‘sparse data extrapolation problem’.

2. METHODS

Data Acquisition

Current capabilities for data collection for experiments involving image-guided liver surgery include the acquisition of: (1) computed tomographic (CT) reconstructed volumes of the tissue/phantom of interest, (2) surface data

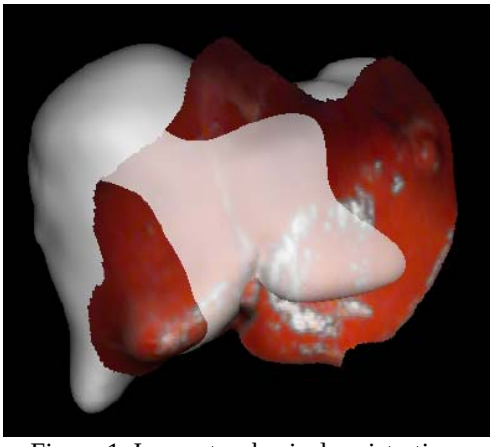

Figure 1. Image-to-physical registration.

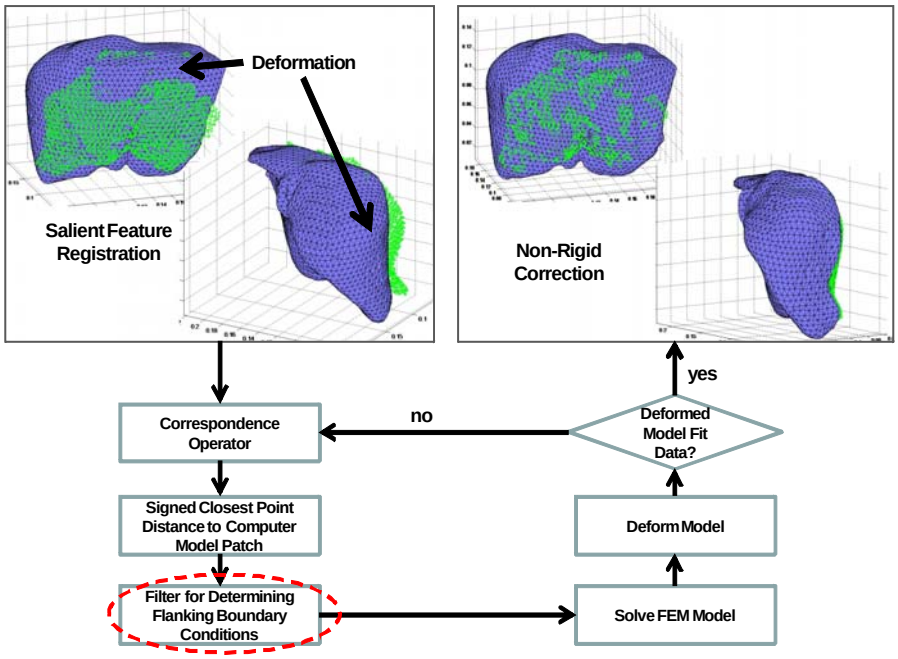

Figure 2. Deformation compensation approach.

in the form of a textured point cloud as provided by a novel optically tracked laser range scanner, and (3) tracked points and contours acquired by an optically tracked stylus. We should note that the textured point cloud is a unique feature to our approach. The laser range scanner passes a laser line over the organ of interest which is detected by a CCD and a 3D point cloud can be generated via triangulation. Using the same CCD (new development see [18]), a color-image of the field of view is recorded and mapped onto the 3D point cloud.

With respect to the current procedural steps for performing image-guided liver surgery, a large incision through the abdomen is created to expose the anterior surface of the liver. Typically either wedge or segmental liver resections are performed to remove one or more hepatic metastases. In wedge resections, the tumor and a 2-3cm surrounding region of the liver is removed, while in segmental resection, an entire anatomic segment of the liver is removed. Prior to the performance of resection, a laser range scanner is brought into the surgical field and a laser range surface of the anterior surface of the liver is acquired. Using the texture information, salient features are identified (falciform ligament, and ridges) and a salient feature registration is executed [13, 19] thus providing a rigid transformation that relates image and physical space. We should also note that a second paradigm is being investigated with respect to this initial registration. Namely, the optically tracked stylus is being used to swab the surface for general surface feature and for the individual salient features. The descriptions are stitched together and a salient feature registration is performed. The pursuit of this direction is in direct response to the 'sparse data extrapolation problem' whereby increased workflow speed could be achieved by a swabbing-only solution.

While this registration has provided some level of guidance, the presence of deformation is evident. Figure 1 is an example of an image-to-physical registration with CT volume rendering shown in gray and the laser range scan of the liver designated by the colored surface. While the surface fit is good, it is clear that shape change between the surfaces has occurred. In this case, the signed distances vary between -12.0 and 12.0 mm across the surface.

Sparse Data Solution Methods

In this paper, we present a comparison among three extrapolative methods that we are investigating towards deformation compensation in the liver. The first extrapolative method among the comparison was presented at SPIE Medical Imaging in 2007 and iteratively fitted an average shape model to the intraoperatively deformed organ [20]. The method was called the iterative closest atlas (ICAt) technique and systematically fit a constructed shape by extracting a weighted combination of pre-computed shapes. This method had the advantage of pre-computing the shapes associated with deformation using a finite element model which allowed for rapid registration intraoperatively. While preliminary

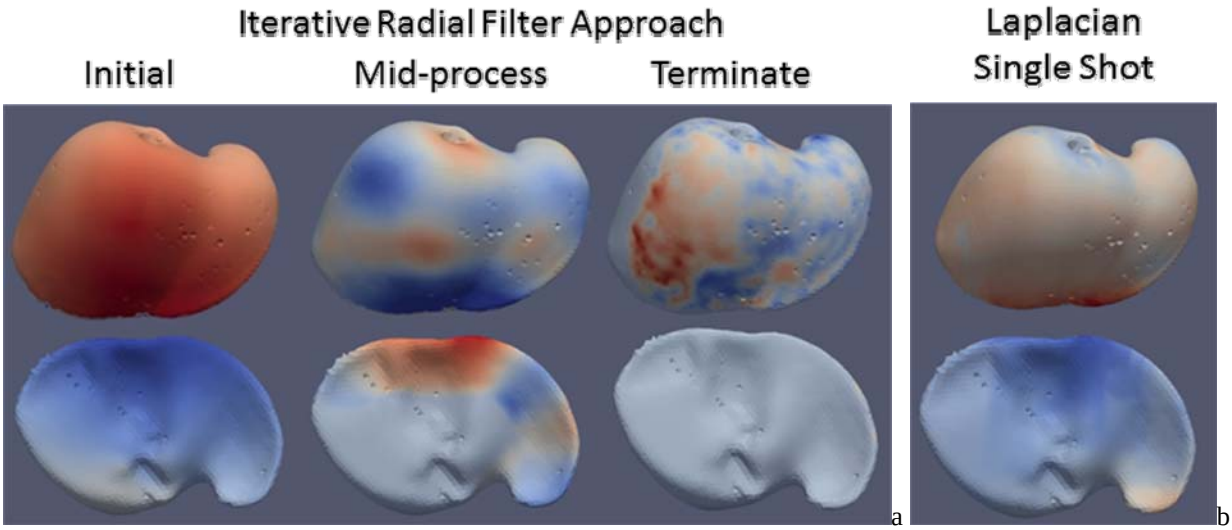

Figure 3. (a) Initial-mid-and last iteration of BC distribution, (b) single iteration with Laplacian methodology. Red indicates displacements applied to model are needed to move along the surface normal while blue indicates moving against the surface normal.

results were encouraging, the atlas shape models were challenging to generate for surgical data. There are still powerful aspects to this work we are investigating.

To compare and complement that previous work, we have explored two sparse data solutions that involve intraoperative computing of our models. Figure 2 is the general form of these methods. The first of these methods was presented at SPIE Medical Imaging in 2010 [21]. In this approach, the correspondence function between laser range scan data (shown as green points in Figure 2) is used to guide the application of boundary conditions similar to work by [22-24]. However, the difficulty in the direct approaches of [22-24] was that sufficient information regarding posterior surfaces needed to be specified which was difficult to approximate, and flanking regions around the laser range scan partial surface were left unmodified which lead to unnatural looking deformations (i.e. a plug-like effect). In the strategy of Figure 2, a spatial surface filter (dashed red line in the figure) that distributes into the flanking regions of the liver surface was created and generated more natural deformations while also having comparable results to the ICAt. The general approach was to generate a radial capture region that was initially quite large (large enough to propagate to the posterior region of the liver). This region would serve as an averaging kernel to distribute the closest-point based boundary condition. With the large kernels, the averaging would result in a small increment of deformation to be applied. As we gradually reduced the kernel size, the liver shape would approach that of the laser range scan. These computations were all compatible with OR timing. We should also note that the radial spatial filter was modified by a norm-sensitizer as it distributed boundary conditions to the posterior side of the liver whereby the boundary conditions would change sign. One advantage of this filter is that it introduces sufficient boundary conditions such that *a priori* assumptions regarding the posterior regions of the liver need not be specified rather the filter approach provides sufficient enhancement to the condition number of matrices associated with FEM calculations to allow for rapid solutions with standard sparse matrix techniques. While this method was comparable to ICAt, the results were of limited success. The last method which is presented here is to use the solution to Laplace's equation along the surface to extrapolate into the flanking regions. We have attempted to use components of this method to assist in non-rigid surface registration of the breast where fiducials are not present [25] and have found reasonable results. Upon completion of the solution of Laplace's equation, the boundary conditions assigned to the posterior regions also undergo a norm-sensed application direction change.

Figure 3 demonstrates the result from the latter two approaches with all surfaces normalized to the max-min range of displacements. Figure 3a illustrates the results at three different iterations associated with the dynamic radial spatial filter method from our technique reported in SPIE 2010. It should be noted that each of iterations shown represents an increment of displacement (typically about 10-15 applied so the per-increment value is quite small in magnitude). Figure 2b shows the single iteration Laplacian method. The Laplacian method is currently executed as

either a single or dual-pass method which makes it considerably faster than the radial method (i.e. only 2 model solves are necessary).

Experimental Methods

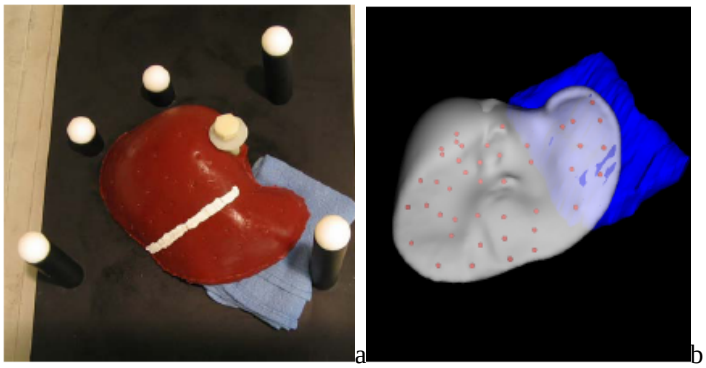

Figure 4. (a) Anthropometric liver phantom with surrounding digitization framework (b) CT rendered surface with applied deformations.

A phantom was constructed from tissue-mimicking material which contained both surface and subsurface beads (N=43) as novel targets (Figure 4). Pre-deformation (2 poses), post-deformation CT images, and laser range scanner data were acquired. Surface-based rigid registrations (iterative closest point – ICP, and salient-feature weighted closest point with partial and full surfaces which we call patch iterative closest point - PICP) were performed. From these initial poses, the three sparse data extrapolative methods were used to correct for subsurface deformation using only the laser range scanned anterior surface data. In addition, a surface-data rich result whereby all geometric surface data (i.e. anterior and posterior) was included was executed for comparison.

In the experiment shown in Figure 4, two deformations (left, and right lobe respectively) were performed and subsurface targets (implanted radio-opaque beads – Figure 4b) were tracked using repeat CT imaging. With both image sets, a series of rigid registrations were employed that involved: (1) affixed fiducials external to the deformation (white balls shown in Figure 4a), (2) iterative closest point registration of before-and-after-deformation anterior surfaces, (3) the salient feature surface registration with anterior surface data only - PICP*, and (4) our salient feature registration with the entire surface (anterior and posterior) - PICP. Once complete the 3 correction frameworks were executed and the respective improvement to correction is reported.

3. RESULTS

Deformation	External Rigid Registration	Organ-Based ICP TRE Mean (Max) Partial Surface	Organ-Based PICP* TRE Mean (Max) Partial Surface	Organ-Based PICP TRE Mean (Max) Full Surface
Left Lobe	14.8±8.5(31.0)	4.4±2.0(10.9)	4.1±2.3(11.3)	3.2±1.5(6.8)
Right Lobe	22.8±8.8(42.3)	4.3±2.0(8.8)	4.5±2.1(10.0)	2.7±1.6(6.7)

Table 1. Rigid registration results for phantom data.

Table 1 shows the target registration error using the rigid-body registration methods. In the first column, the deformation mode is designated. The second column reports the target registration error using external targets (white spheres in Figure 3). The third, fourth, and fifth column reports the target registration error using organ-based ICP, PICP*, and PICP, respectively. The results indicate considerable alignment fidelity by just employing rigid registration based on organ geometry; however, regions of the domain are still misaligned to a significant degree. Table 2 is an analysis of the target registration results using the different correction methods. In Table 2, the first column indicates which deformation state was used for the phantom. The second, third, and fourth columns represent the non-rigid target registration error using the iterative closest atlas (ICAt) technique, the iterative radial filter method, and the novel surface Laplacian solution technique. The top section of the table results are associated with the non-rigid method starting from an initial rigid pose originating from the iterative closest point algorithm (pose associated with 3rd column of Table 1). The bottom results begin from the pose associated with salient feature registration (pose associated with 4th column of

	Initial Pose from ICP		
	ICAt	Radial Spatial BC	Surface Laplacian
Deformation	TRE Mean (Max) [% over PICP*]	TRE Mean (Max) [% over PICP*]	TRE Mean (Max) [% over PICP*]
Left Lobe	4.0±2.6 (14.3) [9.1]	2.6 ± 2.2 (10.0) [40.9]	2.0 ± 1.6 (6.9) [54.5]
Right Lobe	3.3±1.5 (7.4) [23.3]	2.8±2.1 (8.0) [34.9]	2.3 ± 1.6 (6.4) [46.5]
	Initial Pose from PICP		
	ICAt	Radial Spatial BC	Surface Laplacian
Deformation	TRE Mean (Max) [% over PICP*]	TRE Mean (Max) [% over PICP*]	TRE Mean (Max) [% over PICP*]
Left Lobe	2.5±1.1 (5.4) [39]	2.9 ± 2.4 (10.5) [29.3]	2.3 ± 2.1 (8.6) [43.9]
Right Lobe	2.5±1.1 (5.3) [44.4]	3.0±2.1(8.1) [33.3]	2.6 ± 1.9 (8.1) [42.2]

Table 2. Non-rigid results from methods (in mm, bracketed result is in %).

Table 1). There are some aspects to note. Each result has the percent improvement (shown in the brackets) in target error over the rigid salient feature registration method. With the modified approach using the surface Laplacian solution, the improvement level increases to 42-55% of deformation compensation. When realizing that these improvements have been achieved with using sparse anterior surface data only (no intraoperative imaging), this is very encouraging. Another aspect to note with Table 2 is that the results can vary approximately 5-10% based on pose, i.e. the rigid registration pose. Based on this, we will continue to investigate potential rigid registration initial pose algorithms. As far as expectation limits, it would be reasonable to assume that results associated with using the entire surface would likely be the performance limit. Table 3 tabulates these and reports an upper limit to be in the 72-78% correction. We would also like to indicate that all methods are consistent with a 0.5-3 minute update being provided within the OR (ICAt, and Laplacian method being less than 1 minute, while the radial filter method is on the order of 3 minutes).

Deformation	Full Surface BCs TRE Mean (Max) [% over PICP*]
Left Lobe	0.9±0.7 (3.3) [71.9]
Right Lobe	0.6±0.5 (1.8) [77.8]

Table 3. Full surface results (in mm, bracketed result is in %).

4. DISCUSSION

The results shown here demonstrate a comprehensive treatment of the process of deformation correction. It demonstrates that a great deal of error can be corrected by simply doing a rigid body surface registration between the intraoperative organ presentation and its image counterpart acquired preoperatively. The results also indicate that further non-rigid correction can be provided using computational methods, i.e. an approximate reduction in error by half on average in this realization. The results also show that if complete organ surface data could be acquired the deformation correction would rise to a level of approximately 75%. We anticipate that this upper limit is achievable for surgical targets within the focus region for surgery, i.e. usually the region that is presented and laser range scanned (many of the more considerable target errors were with targets that flank the LRS and are remote from the surgical focus).

Another important point is that this algorithmic development has been proposed within the context of the 'sparse data extrapolation problem', i.e. the environment that balances workflow with design, and application with accuracy. The three methods proposed are readily adaptable to the OR environment with minimal interference to the surgeon. The most encumbered is the ICAt whereby preoperative computing has to be conducted prior to surgery. The intraoperative burden on the surgeon is minimal with all 3 methods whereby the only requirements are the acquisition of surface data during surgery. While 100% correction is desirable, even with the use of intraoperative imaging the need to non-rigidly register other preoperative data to the intraoperative image domain would still be a challenge and incur error. In addition, it is not clear that the added 20-30% TRE error remaining would be worth the added encumbrance of an intraoperative CT or MR imaging system. When we examine the cost-effectiveness of the data-rich environment associated with intraoperative imaging in light of the impact to the OR environment as well as the limitations of the actual application of surgery, it is not clear that the accuracy improvements are good solutions to the 'sparse data extrapolation problem'.

5. CONCLUSIONS

This paper proposes solutions to the sparse data extrapolation problem for image-guided liver surgery. The results suggest intraoperative deformation correction from computer models and sparse data to be considerable. This is an important step in the translation of image-guided surgery techniques to the abdomen. Moreover, the algorithms explored are a cost-effective solution that potentially improves the application of surgery, is widely adoptable, and is relatively easy to integrate into current surgical workflow practices. While continued investigation towards improvement is needed, these do represent beneficial advances that can affect the clinical application of surgery today.

6. ACKNOWLEDGEMENTS

This work has been supported by the National Institutes of Health - National Institute of Biomedical Imaging and Bioengineering under grant award R21 EB007694. Dr. Miga is a co-founder and holds ownership interest in Pathfinder Therapeutics Inc. which is currently licensing rights to approaches in image-guided liver surgery.

7. REFERENCES

[1] A. Jemal, R. Siegel, J. Xu, and E. Ward, "Cancer statistics, 2010," *A Cancer Journal for Clinicians*, vol. 60, pp. 1-24, 2010.

[2] A. Jemal, F. Bray, M. M. Center, J. Ferlay, E. Ward, and D. Forman, "Global Cancer Statistics," *CA: A Cancer Journal for Clinicians*, vol. 61, pp. 1-22, 2011.

[3] Y. Fong and L. H. Blumgart, "Surgical options in the treatment of hepatic metastases from colorectal cancer," *Curr. Prob. Surg.*, vol. 35, pp. 336-413, 1995.

[4] R. P. DeMatteo, C. Palese, W. R. Jarnagin, R. L. Sun, L. H. Blumgart, and Y. Fong, "Anatomic segmental hepatic resection is superior to wedge resection as an oncologic operation for colorectal liver metastases," *Journal of Gastrointestinal Surgery*, vol. 4, pp. 178-184, Mar-Apr 2000.

[5] S. Kopetz, G. J. Chang, M. J. Overman, C. Eng, D. J. Sargent, D. W. Larson, A. Grothey, J. N. Vauthey, D. M. Nagorney, and R. R. McWilliams, "Improved Survival in Metastatic Colorectal Cancer Is Associated With Adoption of Hepatic Resection and Improved Chemotherapy," *Journal of Clinical Oncology*, vol. 27, pp. 3677-3683, 2009.

[6] E. Norero, N. Jarufe, J. M. Butte, B. Norero, I. Duarte, J. Torres, G. Pinedo, F. Lopez, J. F. Guerra, L. Ibanez, A. Zuniga, S. Guzman, and J. Martinez, "Outcome of surgical treatment of liver metastasis from colorectal cancer," *Revista Medica De Chile*, vol. 137, pp. 487-496, 2009.

[7] G. Garcea, S. L. Ong, and G. J. Maddern, "Inoperable colorectal liver metastases: A declining entity?," *European Journal of Cancer*, vol. 44, pp. 2555-2572, 2008.

[8] W. R. Jarnagin, M. Gonen, Y. Fong, and e. al., "Improvement in peroperative outcome after hepatic resection: analysis of 1803 consecutive cases over the past decade," *Ann. Surg.*, vol. 236, pp. 397-406, 2002.

[9] C. Laurent, A. Sa Cunha, P. Couderc, and e. al., "Influence of postoperative morbidity on long-term survival following liver resection for colorectal metastases," *Br. J. Surg.*, vol. 90, pp. 1131-1136, 2003.

[10] H. Bruns, K. Kratschmer, U. Hinz, A. Brechtel, M. Keller, M. W. Buchler, and P. Schemmer, "Quality of life after curative liver resection: A single center analysis," *World Journal of Gastroenterology*, vol. 16, pp. 2388-2395, May 2010.

[11] J. Krucker, S. Xu, N. Glossop, A. Viswanathan, J. Borgert, H. Schulz, and B. J. Wood, "Electromagnetic tracking for thermal ablation and biopsy guidance: Clinical evaluation of spatial accuracy," *Journal of Vascular and Interventional Radiology*, vol. 18, pp. 1141-1150, 2007.

[12] D. M. Cash, M. I. Miga, S. C. Glasgow, B. M. Dawant, L. W. Clements, Z. J. Cao, R. L. Galloway, and W. C. Chapman, "Concepts and preliminary data toward the realization of image-guided liver surgery," *Journal of Gastrointestinal Surgery*, vol. 11, pp. 844-859, 2007.

[13] L. W. Clements, W. C. Chapman, B. M. Dawant, R. L. Galloway, and M. I. Miga, "Robust surface registration using salient anatomical features for image-guided liver surgery: Algorithm and validation," *Medical Physics*, vol. 35, pp. 2528-2540, 2008.

[14] T. Lange, N. Papenberg, S. Heldmann, J. Modersitzki, B. Fischer, H. Lamecker, and P. Schlag, "3D ultrasound-CT registration of the liver using combined landmark-intensity information," *International Journal of Computer Assisted Radiology and Surgery*, vol. 4, pp. 79-88, 2009.

[15] O. Heizmann, S. Zidowitz, H. Bourquain, S. Potthast, H. O. Peitgen, D. Oertli, and C. Kettelhack, "Assessment of Intraoperative Liver Deformation During Hepatic Resection: Prospective Clinical Study," *World Journal of Surgery*, vol. 34, pp. 1887-1893, 2010.

[16] T. Lange, T. Wenckebach, H. Lamecker, M. Seebass, M. Hunerbein, S. Eulenstein, and P. M. Schlag, "Registration of portal and hepatic venous phase of MR/CT data for computer-assisted liver surgery planning," *CARS 2005: Computer Assisted Radiology and Surgery*, vol. 1281, pp. 768-772, 2005.

[17] T. Lange, T. H. Wenckebach, H. Lamecker, M. Seebass, M. Hunerbein, S. Eulenstein, B. Gebauer, and P. M. Schlag, "Registration of different phases of contrast-enhanced CT/MRI data for computer-assisted liver surgery planning: Evaluation of state-of-the-art methods," *International Journal of Medical Robotics and Computer Assisted Surgery*, vol. 1, pp. 6-20, 2005.

[18] T. S. Pheiffer, B. Lennon, A. L. Simpson, and M. I. Miga, "Development of a novel laser range scanner," presented at the SPIE Medical Imaging: Visualization, Image-Guided Procedures, and Modeling, Orlando, FL, 2011.

[19] L. W. Clements, D. M. Cash, W. C. Chapman, R. L. Galloway, and M. I. Miga, "Robust surface registration using salient anatomical features in image-guided liver surgery," presented at the SPIE Medical Imaging 2006: Visualization, Image-guided Procedures, and Display, San Diego, CA, 2006.

[20] L. W. Clements, P. Dumpuri, W. C. Chapman, R. L. Galloway Jr., and M. I. Miga, "Atlas-based method for model updating in image-guided liver surgery," presented at the SPIE Medical Imaging 2007: Visualization, Image-Guided Procedures and Display, San Diego, CA, 2007.

[21] P. Dumpuri, L. W. Clements, B. M. Dawant, and M. I. Miga, "Model-updated image-guided liver surgery: preliminary results using intra-operative surface characterization," *SPIE Medical Imaging 2010: Visualization, Image-Guided Procedrues, and Modeling Conference*, vol. 7625, 2010.

[22] D. M. Cash, M. I. Miga, S. C. Glasgow, B. M. Dawant, L. W. Clements, Z. Cao, R. L. Galloway, and W. C. Chapman, "Concepts and preliminary data toward the realization of image-guided liver surgery," *J Gastrointest Surg*, vol. 11, pp. 844-59, Jul 2007.

[23] D. M. Cash, M. I. Miga, T. K. Sinha, R. L. Galloway, and W. C. Chapman, "Compensating for intraoperative soft-tissue deformations using incomplete surface data and finite elements," *IEEE Transactions on Medical Imaging*, vol. 24, pp. 1479-1491, 2005.

[24] M. I. Miga, D. M. Cash, Z. Cao, R. L. Galloway Jr., B. M. Dawant, and W. C. Chapman, "Intraoperative registration of the liver for image-guided surgery using laser range scanning and deformable models," in *Medical Imaging 2003: Visualization, Image-guided Procedures, and Display*, San Diego, 2003, pp. 350-359.

[25] R. E. Ong, J. J. Ou, and M. I. Miga, "Non-rigid registration of breast surfaces using the laplace and diffusion equations," *Biomedical Engineering Online*, vol. 9, 2010.